

Probabilistic reasoning by neurons

Tianming Yang¹ & Michael N. Shadlen¹

Our brains allow us to reason about alternatives and to make choices that are likely to pay off. Often there is no one correct answer, but instead one that is favoured simply because it is more likely to lead to reward. A variety of probabilistic classification tasks probe the covert strategies that humans use to decide among alternatives based on evidence that bears only probabilistically on outcome. Here we show that rhesus monkeys can also achieve such reasoning. We have trained two monkeys to choose between a pair of coloured targets after viewing four shapes, shown sequentially, that governed the probability that one of the targets would furnish reward. Monkeys learned to combine probabilistic information from the shape combinations. Moreover, neurons in the parietal cortex reveal the addition and subtraction of probabilistic quantities that underlie decision-making on this task.

Decision-making is a complicated process that is often based on more than one source of evidence. The brain needs to combine these sources to maximize the chance of achieving a correct decision or to achieve another related goal. Recent advances in neuroscience are beginning to expose the neurobiological mechanisms that underlie simple decisions^{1–6}. It has been demonstrated that, when the outcome of a decision is an eye movement, a neural correlate of the evolving decision can be recorded in brain areas associated with high level motor planning and attention allocation^{7–11}. More specifically, neurons in the lateral intraparietal area (LIP) have been shown to accumulate sensory information provided by earlier visual cortex when a decision is being formed^{8,9,12,13}. The mechanism mimics statistical decision processes that accrue evidence sequentially in the form of a log likelihood ratio (logLR) that favours one outcome over another^{4,14,15}. Therefore, it has been hypothesized that a neuronal substrate of probability integration exists in area LIP¹⁶.

To test this hypothesis, we trained two monkeys to perform a probabilistic categorization task (Fig. 1a). The task was adapted from the well-known weather-prediction task^{17,18} used to study human learning and memory. In each trial the monkey viewed four highly discriminable shapes; these were sampled randomly (with replacement) from a set of ten possible shapes. The shapes were added successively to the display over four half-second epochs. The monkey then made an eye movement to either a red or a green target to receive a reward. Reward was not guaranteed, but was instead governed by a random process based on the combination of preset weights (w) that were assigned to the ten shapes $\{w_1, w_2, \dots, w_{10}\}$. The sum of the four weights associated with the shapes shown in a trial established the log of the odds that reward would accompany a red or a green choice (see Methods Summary).

The large number of possible shape combinations (10^4 permutations; 715 unique combinations) prohibits memorization of specific four-shape patterns and encourages the monkeys to combine evidence from the probabilistic information conferred by each shape in each experimental trial. The optimal strategy is to choose the target with the larger reward probability. However, even when the odds favour red, for example, it is possible that green rather than red will be rewarded. We hoped that the sequential presentation of the shapes would permit a glimpse at how the brain combines probabilities to reach a decision.

Monkeys associated shapes with logLR

After extensive training (see Methods), the monkeys learned to base their decisions on the combined probabilities of the four shapes (Fig. 1b). They chose the red target when the evidence in favour of red was large, and chose the green target when the evidence in favour of green was large (large negative values in Fig. 1b). When the probability was between the two extremes, both monkeys chose either target, but tended to favour the one that was more likely to lead to reward.

To assess the degree to which each shape affected the monkeys' choices, we performed logistic regression (equation (7)), which models the log odds of a red choice as a sum of the weights assigned to each of the four shapes shown in each trial. Logistic regression thus provides a convenient estimate of the leverage that each of the ten shapes exerted on the monkeys' choices; this is given in units of log odds of producing a red choice. These weights, which we term the subjective weight of evidence (subjective WOE), bear a clear resemblance to the weights that were originally assigned to the ten shapes (Fig. 1c; $P < 10^{-5}$ for both monkeys, Spearman's rank correlation test). The rank ordering of the subjective WOE suggests that both monkeys learned the rules of the task, although neither monkey learned the weights perfectly (monkey J was clearly better than monkey H) (see Supplementary Fig. 6 for further analysis of the subjective WOE).

LIP responses are modulated by logLR

We recorded the activity of 64 neurons in the parietal lobe (area LIP) while the monkeys performed the probabilistic classification task. Many neurons in area LIP exhibit spatially selective persistent activity that reliably predicts whether an eye movement is planned into or out of the neuron's response field^{19–22}. The graded activity of these neurons is thought to represent a quantity used by the brain to make simple perceptual decisions^{8,9,11,12,23,24}. We hypothesized that these neural responses encode the logLR that the target in the neuron's response field is the one that will be rewarded.

To test this, we measured the firing rates from these neurons while the monkeys viewed the sequence of shapes that provided them with evidence in favour of reward at the red or green target. In each trial, either the red or the green target was in the neuron's response field (T_{in}). The other target (T_{out}) and the four shapes were placed outside the response field. The logLR is updated with the addition of each of each shape shown in the four presentation epochs. After the n th

¹Howard Hughes Medical Institute, Department of Physiology and Biophysics, National Primate Research Center, University of Washington, Box 357290, Seattle, Washington 98195–7290, USA.

shape (s_n), the WOE is:

$$\text{WOE} \equiv \log \text{LR}_n \equiv \log_{10} \frac{P(s_1, \dots, s_n | \text{reward at } T_{\text{in}})}{P(s_1, \dots, s_n | \text{reward at } T_{\text{out}})} \quad n = \{1, 2, 3 \text{ or } 4\} \quad (1)$$

where $P(x|y)$ denotes the probability of observing x , given that condition y holds true. If the red target is in the neuron's response field, then this value is roughly proportional to the sum of the weights assigned to the n shapes shown in the first n epochs; it equals exactly the sum of the weights once all four shapes are shown ($n = 4$) in the final epoch. The sign is reversed if the green target is in the response

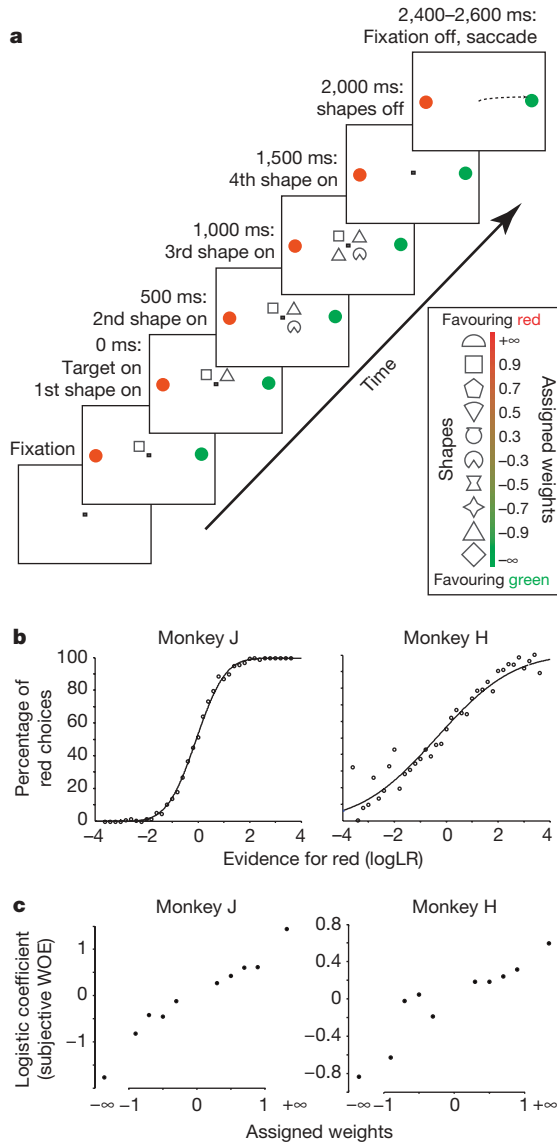


Figure 1 | Probabilistic categorization task. **a**, Task sequence. Four shapes were presented sequentially on the computer monitor near the centre of gaze. After a brief delay period, the monkey made an eye movement (saccade) to either the red or green choice target. During neural recording, one of the choice targets was in the response field of the neuron. The shapes were selected randomly in each trial from a larger set of ten (inset). The reward was determined probabilistically by summing the weights associated with the four shapes. The sum is the logarithm of the odds that the red target will be the one rewarded. **b**, Performance. The fraction of red choices is plotted as a function of the logLR conferred by the four shapes in favour of red. Curves are logistic fits to the data (equation (5)). Only trials that have finite logLR are included in this graph. **c**, Effect of individual shapes on choice. The leverage of each of the ten shapes on the probability of a red choice was inferred using logistic regression. This is the contribution that the shape has on the \log_{10} of the odds of a red choice. These values are plotted as a function of the assigned weights. Standard errors are smaller than the data points in **b** and **c**.

1076

field. In equation (1), one unit of WOE is called a 'ban'²⁵. We next show that LIP neurons modulate their firing rates as a function of these bans of evidence. Not surprisingly, LIP neurons were more responsive near the end of the trials when the monkeys chose T_{in} , as shown by the example neuron in Fig. 2a. The association between

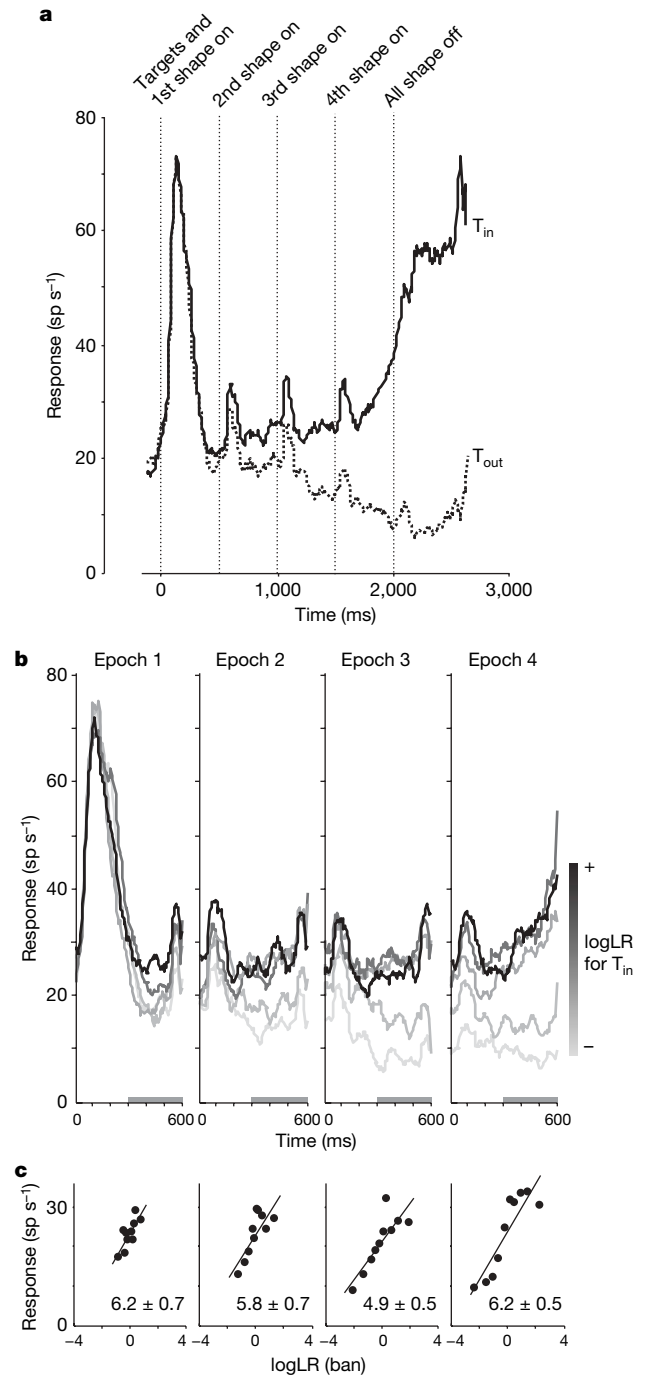


Figure 2 | Responses of an LIP neuron during probabilistic classification. **a**, Evolution of activity. The average firing rate is sorted by the monkeys' choices. The response averages reflect information from shapes shown in all four epochs. Response averages are drawn from 547 T_{in} and 575 T_{out} trials; bin width, 5 ms. **b**, Effect of logLR on firing rate. Response averages are aligned to the onset of the shapes and extend 100 ms into the subsequent epoch. The averages were computed for five quintiles of logLR in each epoch (indicated by shading). Note that a single trial contributes to only one curve in each epoch, but that the quintile can change depending on the sequence of shapes. **c**, Firing rate is affected by logLR. Average firing rate was calculated in the epochs indicated by the grey bars on the x axis of the graphs in **b**. The line is the weighted least-squares fit. The slope (\pm s.e.) provides a modulation index. Sample responses from this neuron can be viewed as Supplementary Movies 1–3.

firing rate and choice is a hallmark of LIP neurons and was nearly guaranteed by our sampling procedure (see Methods). In the present context, the LIP response reveals the outcome of a decision. Far more interesting is the evolution of the response that accompanied the sequential presentation of the shapes. Although a final decision must await the presence of all four shapes, the responses of this neuron were modulated by partial evidence as the shapes appeared in sequence.

The example neuron shown in Fig. 2a responded strongly to the onset of the choice targets that accompanied the first shape. This short latency response is probably caused by the appearance of T_{in} (ref. 26), but by the end of the first epoch the firing rate was affected by one of the ten shapes that appeared near the fixation point. The response was greater for shapes that provided evidence in favour of T_{in} (Fig. 2b). The response curves shown in this epoch sort the 20 possible conditions (10 shapes \times 2 choice target configurations) into quintiles that rank the total logLR for the choice target in the response field. (Note that the logLR quantifies the WOE in favour of T_{in} , regardless of its colour. We use this convention throughout the article for simplicity; but see Appendix C in Supplementary Information.) This difference was even more striking in the second epoch. Again, we grouped the 200 possible conditions (100 possible 2-shape sequences \times 2 choice target configurations) into 5 groups based on the total logLR for reward at T_{in} . The same analysis was performed in the next two epochs. In each epoch, the firing rates are affected by the logLR.

To quantify the effect of logLR on the neural response, we calculated the average firing rate for each trial in the epoch from 300 to

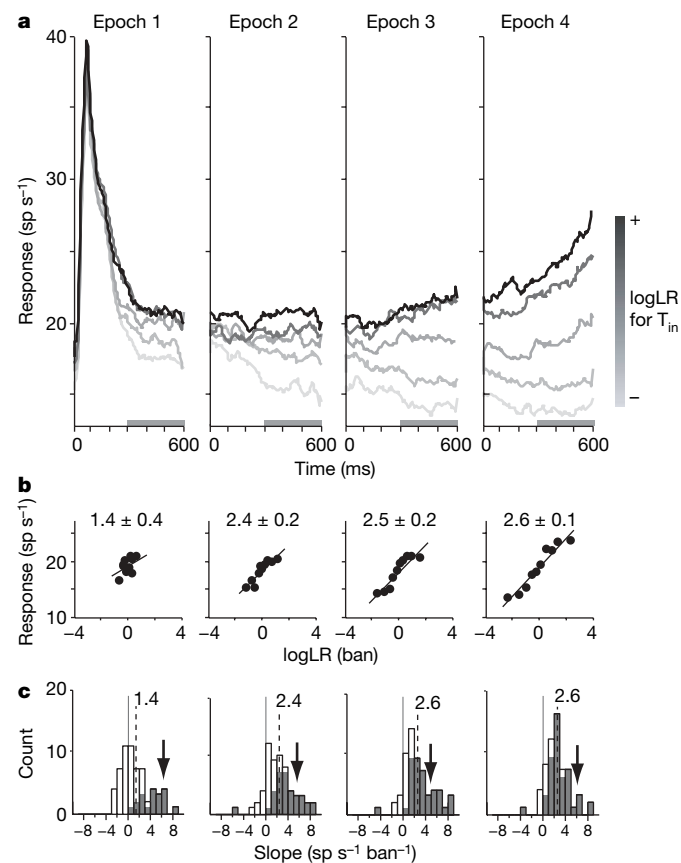


Figure 3 | Population analyses. **a**, Effect of logLR on the population average firing rate, presented in the same format as Fig. 2b (30,930 trials from 64 neurons; bin width, 5 ms). **b**, Firing rate varies linearly with logLR in each epoch, presented in the same format as Fig. 2c. The slope is the best fitting line to the population averages in **a**. **c**, Distribution of modulation indices from all 64 neurons. Indices were derived using the analysis in Fig. 2c. Slopes significantly different from zero are indicated by shaded bars ($P < 0.05$). Dashed lines represent the mean. Arrows indicate the indices for the example neuron in Fig. 2.

600 ms after shape onset, and plotted this value as a function of the logLR (Fig. 2c). The slope of the line of best fit provides an index of the response modulation by logLR and a test of statistical reliability (null hypothesis, H_0 : slope = 0). This neuron exhibited clear modulation of its firing rate as a function of logLR in all epochs ($P < 0.01$). The change in spike rate per ban is indicated in each panel. The positive value implies that the neuron increased its firing rate when the logLR favoured the target in its response field.

We observed a similar pattern of results for the sample of 64 neurons (Fig. 3). The response averages reveal a graded modulation of firing rates that correspond to the magnitude of logLR that favours the target in their response field. When the evidence was against the target in the response field, the population neuronal response decreased. The population average firing rate is well described by a linear function of logLR (Fig. 3b; $P < 0.01$; see equation (8) for $H_0 : b_n = 0$). The modulation indices (in units of spikes per second per ban) are shown for each neuron from the two monkeys (Fig. 3c). Although there is some heterogeneity across the population, the histograms reveal that the change in firing rate per ban is remarkably similar in all four epochs. This finding is supported by data from both monkeys (see Supplementary Fig. 5). In each epoch, LIP registers the appearance of a new shape by adjusting its firing rate to reflect the updated logLR in favour of T_{in} (see Supplementary Movies, which are described briefly in Supplementary Appendix D).

According to this theory, each of the ten shapes should cause a change in LIP activity in accordance with the weight it was assigned. We estimated these changes from the population by attempting to isolate the response to each new shape in each of the four epochs. The responses in the first epoch are obscured by the large visual response accompanying the onset of the choice targets. However, in epochs 2–4, we subtracted the firing rate that the neuron achieved in the previous epoch (see Methods). This procedure yields an estimate of the magnitude and time course of the change in firing rate caused by each of the ten stimuli (Fig. 4).

The shapes caused the firing rate to change with a fairly stereotypical time course, beginning ~ 150 – 200 ms after shape onset without any obvious sign of decay (Fig. 4a). The change in firing rate appears to reflect both the sign and the magnitude of the assigned weights. This is easier to discern from Fig. 4b, which shows the average change in firing

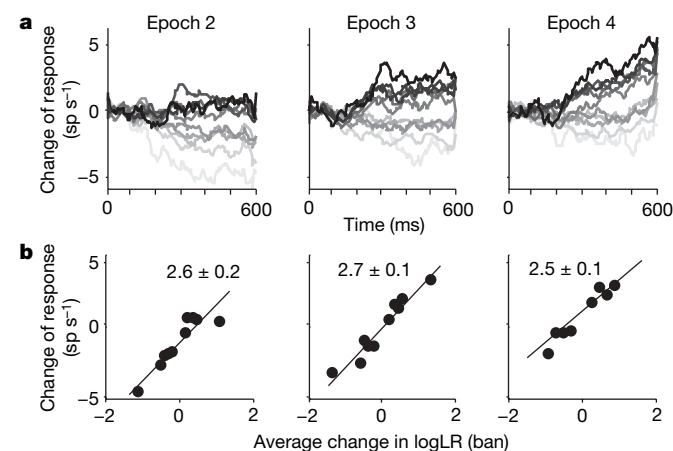


Figure 4 | Effect of individual shapes on LIP activity. The responses are computed by subtracting the firing rate preceding onset of the shape from the recorded value and then averaging the residual perturbations for each shape (see Methods). **a**, Time course of the change in firing rate caused by each of the ten shapes. The darkest curve corresponds to the shape that has the largest weight for T_{in} (semicircle shape when T_{in} is red; diamond shape when T_{in} is green); the lightest line corresponds to the shape that has the largest weight for T_{out} . **b**, The average change of firing rate induced by the ten shapes is plotted as a function of the change in logLR associated with the display of the shape in each of the epochs (Table 1). The two trump shapes are excluded in epoch 4.

rates in the epoch from 300 to 600 ms after shape onset, plotted as a function of logLR. Again, the change in firing rate is proportional to the change in logLR that accompanied addition of the shapes during the trial sequence. The change in spike rate per ban of evidence is similar to the values obtained from the total logLR (Fig. 3b). Furthermore, the changes in firing rate induced by the individual shapes are fairly similar in the three epochs depicted in Fig. 4.

Effect of logLR is not due to shape selectivity or eye movements

At face value, these results indicate that LIP neurons are capable of representing a quantity proportional to logLR. However, two important alternatives deserve consideration: first, LIP neurons might respond to the shapes themselves, independent of the probabilities they confer, and, second, the LIP might simply represent a commitment to move the eyes into or outside of the response field, regardless of the evidence that underlies that plan.

In principle, the observed changes in firing rates could be explained if LIP neurons responded better to some shapes than others^{27,28}. For example, such selectivity could arise as the monkeys learned that some stimuli are more predictive of reward than others^{11,24}. This idea can easily be dismissed. In this investigation, the colour of the target shown in the neuron's response field was randomized from trial to trial. Therefore, each shape combination could furnish evidence in favour either of or against the T_{in} target. In fact, the trials in the first and fifth quintiles in Figs 2b and 3a share the same shape combinations; the same is true for the second and fourth quintiles. Clearly, the responses are not determined by the shapes themselves, but by the bearing the shapes have on the pending decision.

A more serious concern is that the responses are associated with the monkeys' choice rather than with the evidence conferred by the shapes. After all, greater logLR in favour of T_{in} is associated with more neural activity and an increase in the likelihood of an eye movement to the response field. We wished to ascertain whether the effect of logLR on neural response is merely a reflection of the choice made at the end of the trial. In each epoch, we sorted the trials by the choice the monkey made (T_{in} or T_{out}) and subtracted the mean firing rate associated with that choice. The residual firing rates retain a strong dependency on the logLR (Fig. 5a; see also Supplementary Figs 7 and 8). Formally, this analysis is a simple extension of the linear regression depicted in Fig. 3b (see equation (9)). It allows us firmly to reject the hypothesis that the effect of logLR on firing rate is mediated by the eye movement choice ($P < 0.01$ in all epochs, equation (9), $H_0: b_n = 0$). This is true even in the later epochs (T_{out} choices), in which the monkeys' eye movement choice clearly affects the responses. The same analysis performed on individual neurons also supports this conclusion: 84%, 76%, 60% and 28% of neurons in which logLR had significant effects on firing rate (epochs 1–4, respectively; filled bars in Fig. 3c) retained this significance when we controlled for choice ($P < 0.05$, equation (9)).

Table 1 | Change in logLR conferred by the ten shapes in each epoch

Shapes	$\Delta \log LR$ (ban)			
	Epoch I	Epoch II	Epoch III	Epoch IV
 	± 1.09	± 1.31	± 1.67	–
 	± 0.32	± 0.37	± 0.49	± 0.9
 	± 0.25	± 0.30	± 0.39	± 0.7
 	± 0.18	± 0.21	± 0.28	± 0.5
 	± 0.11	± 0.12	± 0.17	± 0.3

Values for epochs II–IV are averages, which take into account all possible shape combinations in the preceding epochs. The sign of the change depends on whether the red or green target is in the neuron's response field. The change in logLR is not meaningful in epoch 4 for the trump shapes because the majority of combinations result in $\pm \infty$. For the same shapes, there are 18 combinations in epoch III that result in $\pm \infty$; these are excluded from this average.

The preceding analysis indicates that the monkeys' choice does not explain the effect of logLR on firing rate, but it is possible that the monkey favours one choice or the other in each epoch and simply changes this binary commitment in the subsequent epoch upon acquisition of new information. This idea could explain the weak effect of choice on neural response in early epochs while leaving open the possibility that logLR is not in fact represented. According to this formulation, the intermediate levels of activity that appear to correspond to different levels of logLR are actually mixtures of responses associated with just two 'states' of commitment, albeit temporary.

To test for this possibility, we measured the variance in firing rates across trials. If intermediate levels of firing are mixtures of high and low firing rate states, then the variance should be predicted by sampling responses from the distributions of responses associated with the highest and lowest quintiles (grey curves, Fig. 5b; see Methods). In contrast, if the intermediate firing rates represent actual firing rate modes, the variance should be approximately proportional to the mean firing rate^{29–31}, corresponding to straight lines in Fig. 5b. This analysis firmly rejects the conjecture that the intermediate firing rates are actually mixtures of trials drawn from the extreme quintiles (H_0 : mixture; $P < 0.01$ in the four shape epochs, F -test). It provides clear evidence that the intermediate firing rates represent a graded quantity that is proportional to logLR. In fact, a significant deviation from a graded representation of logLR (straight lines in Fig. 5b) is only observed in the fourth epoch and in the delay period (H_0 : non-mixture; $P < 0.01$), when a categorical decision is expected.

Together, the analyses in Fig. 5 indicate that the LIP activity represents both the outcome of the decision process—an eye movement—and the accumulated evidence on which this decision is based. The evidence in the form of logLR affects both LIP firing rates and the choice. In early epochs the firing rates are predominantly affected by the logLR, whereas in later epochs the rates are associated with both logLR and choice. Note, however, that the effect of logLR on firing rate is nearly the same in all epochs (Fig. 3b); it is also the same for the individual shapes (Fig. 4b). Therefore, even in the later epochs when

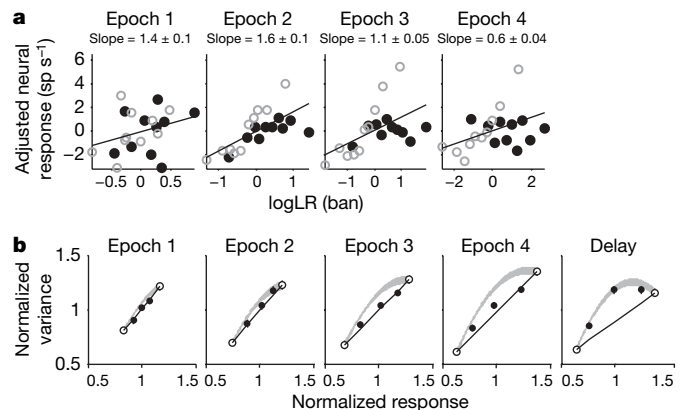


Figure 5 | The effect of logLR on firing rate is not explained by motor

planning. **a**, Analysis of the potential confounding effect of eye movement. Data points are mean values of adjusted firing rates, detrended for the effect of eye movement at the end of the trial. Detrending was achieved for each cell and in each epoch by subtracting the mean firing rate for T_{in} or T_{out} choices from the firing rate in single trials. Lines are based on fits to equation (9) ($\text{slope} = b_n$) using all trials in each epoch ($N \approx 21,000$ to 30,000). Slopes (\pm s.e.) are in units of spikes per second per ban. For the purpose of display, points represent ten divisions of logLR ($\sim 1,500$ trials per point). Filled circles, T_{in} choices; open circles, T_{out} choices. **b**, Rejection of a mixture model. Graphs show the relationship between the mean firing rate and variance for five quintiles of logLR in a 300 ms window in each epoch (see Methods) and in the delay period (300 ms presaccadic interval). The values are normalized for each neuron and are averaged to produce the points shown (error bars are s.e.m.; $n = 64$ neurons). The grey line shows the predicted variance (\pm s.e.) if the intermediate levels of firing rate were composed of mixtures of firing rate states associated with the lowest and highest quintiles (open symbols).

the firing rates are dominated by the monkeys' ultimate choice (Supplementary Fig. 7), parsimony suggests that logLR causes a change in LIP firing rate, which in turn causes (or is associated with) a change in the probability of a T_{in} choice.

LIP reflects behavioural variations not explained by logLR

To date, we have focused our analyses on the relationship between neural response and the actual logLR conferred by the ten shapes. Although the monkeys learned these probabilistic relationships, they were not perfect. As shown in Fig. 2, the leverage that the ten shapes exerted on behaviour, termed the subjective WOE, was different between the two monkeys and exhibited some departures from the scaling imposed by the assigned weights. We wondered whether LIP activity is correlated with these idiosyncrasies. To test this, we conducted a nested regression analysis, which was designed to reveal whether knowledge of the discrepancies between logLR and the subjective WOE could explain some of the remaining variance in neural responses (see Methods). For all four epochs tested in both monkeys, knowledge of subjective WOE improved the regression significantly ($P < 0.005$, equation (10), $H_0 : d_n = 0$). We conclude that LIP neurons encode the systematic biases formed by the monkeys in the association of shape and evidence bearing on the decision.

In addition to these systematic biases, the LIP recordings help to explain why the monkeys vary their choices even when faced with the same evidence (for example, Supplementary Fig. 2a). The variation in firing rate from a single neuron has a detectable effect on the choices the monkey makes: on average, a variation of 1 spike per second from a single neuron was equivalent to ~ 0.1 ban of evidence ($P < 0.05$ for all but the first epoch for both monkeys; see equations (11) and (12)). Such correlations are thought to arise because the variability in firing rate from single neurons is shared to a small degree with other neurons that underlie the choice^{31–33}. Thus, the mechanism underlying probabilistic behaviour in our task resembles the mechanism underlying errors on difficult perceptual tasks when evidence is weak—that is, signals that affect behaviour are often contaminated by noise.

Discussion

Humans make probabilistic classifications in a variety of settings in which information bears on—but does not guarantee—an outcome. In the weather-prediction task, for example, a human is asked to predict the weather based on a set of cards with symbols on them. Like our shapes, these symbols possess probabilistic associations with the possible outcomes (rain or sunshine), and the subject receives feedback on his or her decision. This task is thought to rely on procedural memory circuits that involve the basal ganglia during learning³⁴. Although we cannot be sure that the monkeys in this investigation use the same strategy as humans, this study begins to raise questions about the connection between so-called habit learning and cortical computations associated with probabilistic inference. The capacity to train monkeys on this task opens new possibilities for further investigations.

As has been found in other decision-making tasks, when a decision is ultimately expressed through a movement, neurons in high-level command structures of the brain mediate the logical connection between evidence and plan of action^{8,11,23,35–38}. As in simple decisions, this evolution of the LIP response represents the accumulation of evidence leading to commitment to a behavioural choice³⁹. Indeed, it has been suggested that the build-up of activity in the brain associated with a wide variety of simple decisions is an approximation to the summation of logarithms of probabilities, likelihoods, odds, and so on^{16,40–44}. The present findings provide direct confirmation of these theoretical insights for the first time. They demonstrate directly that the firing rates of LIP neurons are proportional to the logLR conferred by the shape stimuli in our task.

This interpretation does not exclude the possibility that LIP encodes many other useful quantities for decision-making (for example, value, utility or reward expectation^{11,24,45}), especially if the encoding is in

units roughly proportional to logLR⁴⁶. Even in this study, there are alternatives to the logLR that would produce similar results. For example, the brain might approximate the logLR associated with each shape on the assumption of conditional independence—in essence, that the logLR for epoch 1 holds for all epochs, what we term 'naive WOE'. This quantity would be easy to estimate from the frequency of observing each shape in association with reward at the red and green targets. It has the virtue of simplicity, and it predicts the pattern of response seen with the two 'trump' shapes (half-circle and diamond; see Supplementary Appendix A). A related alternative is the subjective WOE—the quantity we derived from our behavioural analysis (Fig. 1c). Not only is subjective WOE approximately proportional to the logLR but also it reflects the systematic error in the monkeys' choices. Indeed, we would have obtained similar results in all analyses in this article if we substituted subjective WOE for logLR. We presented the results of behavioural measurements and neural recordings as a function of logLR because that is the experimentally controlled independent variable. Thus, we have established a link between logLR and both neural activity and choice.

We do not know how the brain converts information about shape into a number proportional to logLR, and we do not know whether area LIP plays a role in this transformation or whether it represents only the outcome of this conversion. Presumably, neurons in ventral stream visual areas play a role in discriminating the shapes⁴⁷, but how their responses are converted to a logLR value is not known. In a motion-discrimination task it has been shown that LIP neurons represent the accumulated difference in firing rates from direction-selective neurons with opposing direction preferences^{13,48}. This difference approximates a logLR^{43,49}. It remains to be seen whether a similar readout of ventral stream neurons occurs in our probabilistic classification task.

Although designed to test a straightforward hypothesis about a particular representation of probability, the present study exposes the brain's capacity to extract probabilistic information from a set of symbols and to combine this information over time. Thus, we have demonstrated a crude capacity for probabilistic inference in monkeys—a capacity that might underlie cognitive reasoning in humans.

METHODS SUMMARY

Two monkeys (*Macaca mulatta*) were trained in a probabilistic categorization task (Fig. 1). In each trial, the monkey maintained its gaze at a fixation point. Two choice targets (red and green) were displayed in opposite hemifields (eccentricity range 8° to 12°). Next, four shapes were presented at regular 500 ms intervals. The four shape positions (0.5° from the fixation point) were displayed in a random order in each trial. The shapes were erased 500 ms after onset of the fourth. A memory delay period (450–550 ms) preceded offset of the fixation point, which instructed the monkey to make an eye movement to one of the choice targets. A liquid reward was administered probabilistically for either the red or green choice, as described below.

Each shape was drawn randomly from a pool of ten shapes (sampled with replacement). We assigned each shape a unique weight: $\{w_1, w_2, \dots, w_{10}\} = \{-\infty, -0.9, -0.7, -0.5, -0.3, +0.3, +0.5, +0.7, +0.9, +\infty\}$. The extreme weights, which we term 'trumps', can be regarded as a pair of very large numbers, $w_1 = \lim_{x \rightarrow \infty} (-x)$, $w_{10} = \lim_{x \rightarrow \infty} (x)$, which cancel when they appear together. The sum of the weights associated with the four shapes governed the probability that a red (R) or a green (G) choice would be rewarded.

$$P(R|s_1, s_2, s_3, s_4) = \frac{\sum_{i=1}^4 w_i}{10 + \sum_{i=1}^4 w_i} \quad (2)$$

$$P(G|s_1, s_2, s_3, s_4) = 1 - P(R|s_1, s_2, s_3, s_4)$$

where s_i represents the shape shown in the i th epoch. The sum of weights is the log of the posterior odds in favour of red.

$$\log_{10} \frac{P(R|s_1, s_2, s_3, s_4)}{P(G|s_1, s_2, s_3, s_4)} = \sum_{i=1}^4 w_i \quad (3)$$

The computer controlled the reward using $P(R|s_1, s_2, s_3, s_4)$.

We recorded extracellularly from single neurons in LIP while the monkeys performed the task with one of the choice targets (T_{in}) in the neuron's response field. Neither T_{out} nor the shapes were near the neuron's response field. We selected all well isolated neurons that had spatially selective persistent activity during a memory delay period⁵⁰. A total of 64 neurons were recorded for at least 100 trials and were included in our analysis (45 and 19 from monkeys J and H, respectively). See Methods for further details.

All experimental procedures were performed in accordance with the NIH Guide for the Care and Use of Laboratory Animals and were approved by the University of Washington Animal Care Committee.

Full Methods and any associated references are available in the online version of the paper at www.nature.com/nature.

Received 30 November 2006; accepted 18 April 2007.

Published online 3 June 2007.

- Schall, J. D. Neural correlates of decision processes: neural and mental chronometry. *Curr. Opin. Neurobiol.* **13**, 182–186 (2003).
- Glimcher, P. W. The neurobiology of visual-saccadic decision making. *Annu. Rev. Neurosci.* **26**, 133–179 (2003).
- Horowitz, G. D., Batista, A. P. & Newsome, W. T. Representation of an abstract perceptual decision in macaque superior colliculus. *J. Neurophysiol.* **91**, 2281–2296 (2004).
- Gold, J. I. & Shadlen, M. N. Banburismus and the brain: decoding the relationship between sensory stimuli, decisions, and reward. *Neuron* **36**, 299–308 (2002).
- Romo, R., Hernandez, A. & Zainos, A. Neuronal correlates of a perceptual decision in ventral premotor cortex. *Neuron* **41**, 165–173 (2004).
- Barlow, H. Conditions for versatile learning. Helmholtz's unconscious inference, and the task of perception. *Vision Res.* **30**, 1561–1571 (1990).
- Gold, J. I. & Shadlen, M. N. The influence of behavioral context on the representation of a perceptual decision in developing oculomotor commands. *J. Neurosci.* **23**, 632–651 (2003).
- Roitman, J. D. & Shadlen, M. N. Response of neurons in the lateral intraparietal area during a combined visual discrimination reaction time task. *J. Neurosci.* **22**, 9475–9489 (2002).
- Shadlen, M. N. & Newsome, W. T. Neural basis of a perceptual decision in the parietal cortex (area LIP) of the rhesus monkey. *J. Neurophysiol.* **86**, 1916–1936 (2001).
- Kim, J. N. & Shadlen, M. N. Neural correlates of a decision in the dorsolateral prefrontal cortex of the macaque. *Nature Neurosci.* **2**, 176–185 (1999).
- Platt, M. L. & Glimcher, P. W. Neural correlates of decision variables in parietal cortex. *Nature* **400**, 233–238 (1999).
- Hanks, T. D., Ditterich, J. & Shadlen, M. N. Microstimulation of macaque area LIP affects decision-making in a motion discrimination task. *Nature Neurosci.* **9**, 682–689 (2006).
- Huk, A. C. & Shadlen, M. N. Neural activity in macaque parietal cortex reflects temporal integration of visual motion signals during perceptual decision making. *J. Neurosci.* **25**, 10420–10436 (2005).
- Link, S. W. & Heath, R. A. A sequential theory of psychological discrimination. *Psychometrika* **40**, 77–105 (1975).
- Wald, A. *Sequential Analysis* (Wiley, New York, 1947).
- Gold, J. I. & Shadlen, M. N. The neural basis of decision making. *Annu. Rev. Neurosci.* **30**, 535–574 (2007).
- Knowlton, B. J., Mangels, J. A. & Squire, L. R. A neostriatal habit learning system in humans. *Science* **273**, 1399–1402 (1996).
- Gluck, M. A., Shohamy, D. & Myers, C. How do people solve the “weather prediction” task?: individual variability in strategies for probabilistic category learning. *Learn. Mem.* **9**, 408–418 (2002).
- Gnadt, J. W. & Andersen, R. A. Memory related motor planning activity in posterior parietal cortex of monkey. *Exp. Brain Res.* **70**, 216–220 (1988).
- Platt, M. L. & Glimcher, P. W. Responses of intraparietal neurons to saccadic targets and visual distractors. *J. Neurophysiol.* **78**, 1574–1589 (1997).
- Colby, C. L. & Goldberg, M. E. Space and attention in parietal cortex. *Annu. Rev. Neurosci.* **22**, 319–349 (1999).
- Ipata, A. E., Gee, A. L., Goldberg, M. E. & Bisley, J. W. Activity in the lateral intraparietal area predicts the goal and latency of saccades in a free-viewing visual search task. *J. Neurosci.* **26**, 3656–3661 (2006).
- Leon, M. I. & Shadlen, M. N. Representation of time by neurons in the posterior parietal cortex of the macaque. *Neuron* **38**, 317–327 (2003).
- Sugrue, L. P., Corrado, G. S. & Newsome, W. T. Matching behavior and the representation of value in the parietal cortex. *Science* **304**, 1782–1787 (2004).
- Good, I. J. Studies in the history of probability and statistics. XXXVII A.M. Turing's statistical work in World War II. *Biometrika* **66**, 393–396 (1979).
- Bisley, J. W., Krishna, B. S. & Goldberg, M. E. A rapid and precise on-response in posterior parietal cortex. *J. Neurosci.* **24**, 1833–1838 (2004).
- Sereno, A. B. & Maunsell, J. H. Shape selectivity in primate lateral intraparietal cortex. *Nature* **395**, 500–503 (1998).
- Sereno, A. B. & Amador, S. C. Attention and memory-related responses of neurons in the lateral intraparietal area during spatial and shape-delayed match-to-sample tasks. *J. Neurophysiol.* **95**, 1078–1098 (2006).
- Tolhurst, D. J., Movshon, J. A. & Dean, A. F. The statistical reliability of signals in single neurons in cat and monkey visual cortex. *Vision Res.* **23**, 775–785 (1983).
- Geisler, W. S. & Albrecht, D. G. Visual cortex neurons in monkeys and cats: detection, discrimination and identification. 897–920 (1997).
- Shadlen, M. N. & Newsome, W. T. The variable discharge of cortical neurons: implications for connectivity, computation, and information coding. *J. Neurosci.* **18**, 3870–3896 (1998).
- Zohary, E., Shadlen, M. N. & Newsome, W. T. Correlated neuronal discharge rate and its implications for psychophysical performance. *Nature* **370**, 140–143 (1994); erratum **371**, 6495 (1994).
- Parker, A. J. & Newsome, W. T. Sense and the single neuron: probing the physiology of perception. *Annu. Rev. Neurosci.* **21**, 227–277 (1998).
- Knowlton, B. J., Squire, L. R. & Gluck, M. A. Probabilistic classification learning in amnesia. *Learn. Mem.* **1**, 106–120 (1994).
- Gold, J. I. & Shadlen, M. N. Representation of a perceptual decision in developing oculomotor commands. *Nature* **404**, 390–394 (2000).
- Cisek, P. & Kalaska, J. F. Neural correlates of reaching decisions in dorsal premotor cortex: specification of multiple direction choices and final selection of action. *Neuron* **45**, 801–814 (2005).
- Wise, S. P. & Murray, E. A. Role of the hippocampal system in conditional motor learning: mapping antecedents to action. *Hippocampus* **9**, 101–117 (1999).
- Sugrue, L. P., Corrado, G. S. & Newsome, W. T. Choosing the greater of two goods: neural currencies for valuation and decision making. *Nature Rev. Neurosci.* **6**, 363–375 (2005).
- Smith, P. L. & Ratcliff, R. Psychology and neurobiology of simple decisions. *Trends Neurosci.* **27**, 161–168 (2004).
- Jazayeri, M. & Movshon, J. A. Optimal representation of sensory information by neural populations. *Nature Neurosci.* **9**, 690–696 (2006).
- Carpenter, R. & Williams, M. Neural computation of log likelihood in control of saccadic eye movements. *Nature* **377**, 59–62 (1995).
- Holmes, P. *et al.* Optimal decisions: from neural spikes, through stochastic differential equations, to behavior. *IEICE Trans. Fundamentals* **88**, 2496–2503 (2005).
- Gold, J. I. & Shadlen, M. N. Neural computations that underlie decisions about sensory stimuli. *Trends Cogn. Sci.* **5**, 10–16 (2001).
- Ma, W. J., Beck, J. M., Latham, P. E. & Pouget, A. Bayesian inference with probabilistic population codes. *Nature Neurosci.* **9**, 1432–1438 (2006).
- Dorris, M. C. & Glimcher, P. W. Activity in posterior parietal cortex is correlated with the relative subjective desirability of action. *Neuron* **44**, 365–378 (2004).
- Green, D. M. & Swets, J. A. *Signal Detection Theory and Psychophysics* (John Wiley and Sons, New York, 1966).
- Tanaka, K. Inferotemporal cortex and object vision. *Annu. Rev. Neurosci.* **19**, 109–139 (1996).
- Ditterich, J., Mazurek, M. & Shadlen, M. N. Microstimulation of visual cortex affects the speed of perceptual decisions. *Nature Neurosci.* **6**, 891–898 (2003).
- Shadlen, M. N., Hanks, T. D., Churchland, A. K., Kiani, R. & Yang, T. in *Bayesian Brain: Probabilistic Approaches to Neural Coding* (eds Doya, K., Ishii, S., Rao, R. & Pouget, A.) 209–237 (MIT Press, Cambridge, 2006).
- Hikosaka, O. & Wurtz, R. H. Visual and oculomotor functions of monkey substantia nigra pars reticulata. III. Memory-contingent visual and saccade responses. *J. Neurophysiol.* **49**, 1268–1284 (1983).

Supplementary Information is linked to the online version of the paper at www.nature.com/nature. A summary figure is also included.

Acknowledgements We thank H. Brew, A. Churchland, T. Hanks, R. Kiani and J. Palmer for advice and comments, M. Mihali and V. Skypceck for technical assistance, and M. McKinley for preparing movie demonstrations. This work was supported by the Howard Hughes Medical Institute (HHMI) and grants from the NEI and NCR. R.

Author Contributions The authors designed the project together. T.Y. collected data and performed the data analysis. T.Y. and M.N.S. wrote the paper.

Author Information Reprints and permissions information is available at www.nature.com/reprints. The authors declare no competing financial interests. Correspondence and requests for materials should be addressed to T.Y. (tianming@u.washington.edu) or M.N.S. (shadlen@u.washington.edu).

METHODS

Here we describe important details about the behavioral and physiological methods used in this study. We also explain the analyses described in the main text.

Task. In each trial, the monkey maintained its gaze within $\pm 1^\circ$ of a fixation point (0.2° in diameter) centred on the video monitor. After a variable delay, two choice targets (red and green) were displayed in opposite hemifields (eccentricity range 8° to 12° ; median 10°). At the same time (monkey J) or 500 ms later (monkey H), the first of four shape-stimuli appeared near the fixation point. Next, shapes 2, 3 and 4 were presented at regular 500 ms intervals. Each shape was randomly drawn from a pool of ten shapes (probability 0.1; sampled with replacement). The four positions (0.5° from the fixation point) were assigned in random order in each trial. The shapes were drawn as white lines on a black background (line length 2° ; thumb print $<(0.5^\circ)^2$; Fig. 1). The shapes were erased 500 ms after onset of the fourth. A memory delay period (450–550 ms) preceded the removal of the fixation point, which instructed the monkey to make an eye movement to one of the choice targets. A liquid reward was administered probabilistically for either the red or the green choice, as described below.

Training. Animals were seated comfortably in a primate chair with their head fixed. Eye position was monitored using a scleral search coil (CNC Engineering)⁵¹. Horizontal and vertical eye positions were sampled at 500 Hz using the NIH Rex system⁵². Both animals had received prior training on delayed eye-movement tasks. We began training with a one-shape version of the categorization task. We first used the shapes with $w = \pm \infty$, for which the ‘correct’ choice would yield reward with 100% certainty. Once animals consistently achieved at least 70% correct choices, we enlarged the pool of possible test shapes using the pair of shapes that had the next largest weights. Reward was administered probabilistically for these new shapes (using a variant of equation (2) with just one term in the sum), but we kept track of the fraction of trials in which the monkey chose the target that was favoured by the weights, even if the choice did not pay off. When the monkey reached 70% correct choices, we added the third pair of shapes, and so on. Here, correct means the choice of the target that has larger reward probability.

Once the monkey learned this one-shape version of the task (ten and four weeks for monkeys J and H, respectively), we began training on the n -shape version of the task. We provided only minimal exposure to versions of the task that had two and three shapes (two and one weeks for monkeys J and H, respectively), because, to our surprise, the monkeys were willing to perform the four-shape version without these intervening steps. Monkey J underwent 8 weeks of training in the full four-shape version of the task ($\sim 130,000$ trials). By the first recording session, this monkey was choosing the better reward target in more than 85% of trials. Monkey H received 10 weeks of training on the full 4-shape version of the task ($\sim 134,000$ trials). Because a veterinary complication (endometriosis) favoured an expedited testing schedule, we started recording when this monkey chose the better reward target in $\sim 75\%$ of trials.

Recording. We recorded extracellularly from single neurons in area LIP while the monkeys performed the task. We targeted neurons in the posterior third of the ventral division of LIP^{53,54} by registering recording locations estimated from our magnetic resonance imaging studies (Supplementary Fig. 4a) to a high resolution scan supplied with the Caret atlas⁵⁵ (<http://brainmap.wustl.edu/caret>). A hydraulic microdrive mounted over the cylinder advanced the electrodes to the desired depth (FHC, <http://www.fh-co.com/>). Spikes from individual neurons were isolated using a dual voltage–time window discriminator (Bak Electronics). They were recorded with a resolution of 1 ms for off-line analysis using custom software written in Matlab (Mathworks). We screened neurons using a simple delayed eye-movement paradigm^{50,56}. We selected for further study all well isolated neurons that had spatially selective persistent activity during the memory delay period (500–1,000 ms) between target flash and an eye movement to its remembered location ($\pm 2.5^\circ$) (ref. 50). Neurons that have this property are abundant in the ventral division of LIP⁵⁶.

Data analysis. The main independent variable in this study is the WOE conferred by the sequence of shapes ($\log LR_m$, equation (1)). Bayes’ rule ensures that this is equal to the log of the posterior odds (equation (3)) once all four shapes are shown. This is because the prior probability of reward at red (R) is equal to the prior probability of reward at green (G):

$$\log_{10} \frac{P(s_1, s_2, s_3, s_4 | R)}{P(s_1, s_2, s_3, s_4 | G)} = \log_{10} \frac{P(R | s_1, s_2, s_3, s_4)}{P(G | s_1, s_2, s_3, s_4)} = \sum_{i=1}^4 w_i \quad (4)$$

The $\log LR$ from partial evidence (that is, fewer than four shapes) was calculated by tabulating the expected frequencies of reward associated with each shape combination, rather than the partial sums of weights. For an explanation of the difference between these two approaches, see Supplementary Appendices A and B. To calculate the $\log LR$ associated with a particular shape in each epoch

(Table 1), we averaged the change in $\log LR$ conferred by the shape; this was done for all possible shape combinations in the preceding epochs, excluding the appearance of the trump shapes when they guaranteed reward at red or green (that is, an unbalanced trump in the fourth epoch and the rare run of two or more unbalanced trumps in epoch three).

Analyses of behavioural data. We used a variety of logistic models to ascertain the effect of the shape combinations on choice. The sigmoid in Fig. 1b is described by

$$P_{\text{red}} = \frac{10^Q}{1 + 10^Q} \quad \text{where } Q = \beta_0 + \beta_1 \log_{10} \frac{P(s_1, s_2, s_3, s_4 | R)}{P(s_1, s_2, s_3, s_4 | G)} \quad (5)$$

where the β_i are fitted coefficients (method of maximum likelihood assuming the Bernoulli distribution of binary choices). Nearly identical results are obtained by replacing the $\log LR$ in equation (5) by the sum of the four weights or by an alternative to the $\log LR$, termed naive WOE, described in the Appendix A of the Supplementary Information. We use equation (5) for consistency with other analyses for which WOE (as defined in equation (1)) is the only mathematically correct option (see Supplementary Appendix A). The trials that used infinite total weights were not included in this analysis. In these trials, we assessed the leverage of shapes that have finite weight on choice by letting

$$P_{\text{red}} = \frac{10^Q}{1 + 10^Q} \quad \text{where } Q = \gamma_0 + \gamma_1 \sum_{i=1}^3 w_i \quad (6)$$

where the w_i are the weights assigned to the three shapes that have finite weight. We performed this test separately for the two trump shapes. The null hypothesis is that the three shapes that have finite weight do not affect choice in the presence of a trump shape (Supplementary Fig. 2b).

To estimate the effect of individual shapes on the monkeys’ choices, we incorporated a term for each of the ten possible shapes in the logistic regression:

$$P_{\text{red}} = \frac{10^{Q^*}}{1 + 10^{Q^*}} \quad \text{where } Q^* = \sum_{j=1}^{10} w_j^* N_j \quad (7)$$

and the N_j are the counts for each shape type presented in a trial. The ten fitted coefficients w_j^* are the subjective WOE. Subscript j in this equation refers to shape (see also Supplementary Fig. 6).

Analyses of physiological data. Our primary analyses test the relationship between the $\log LR$ associated with shape sequences and the neuronal firing rate. For most analyses, firing rates were estimated in single trials in each of the four shape epochs from 300–600 ms after shape onset. Responses tended to be stable in this interval and were uncontaminated by onset of choice targets (first epoch) or the subsequent shape (epochs two and three). None of the results in this article rest critically on the definition of this epoch. Although many graphs display data grouped by $\log LR$ (quintiles, running means and binned data), all fits and statistical tests were performed using individual trials rather than mean responses, unless otherwise noted. Fits to individual trials used least squares, and fits to means (and their s.e.) used weighted least squares.

For the analyses in Figs 2 and 3, we used simple linear regression in each epoch:

$$y_n = a_n + b_n \log LR_n \quad (8)$$

where y_n is the firing rate (in each trial) in epoch n , and $\log LR_n$ is given by equation (1). The fitted coefficients, a and b , are the intercept and slope of the line, respectively. We refer to the latter as a modulation index for the neuron or the population.

To test whether the effect of $\log LR$ is explained by the eye movement made at the end of the trial, we added a third term to this equation:

$$y_n = a_n + b_n \log LR_n + c_n I_{\text{eye}}, \quad I_{\text{eye}} = \begin{cases} 1 & \text{if eye movement is to } T_{\text{in}} \\ 0 & \text{if eye movement is to } T_{\text{out}} \end{cases} \quad (9)$$

The null hypothesis is that the effect of $\log LR$ on LIP response is explained by the eye movement ($H_0: b_n = 0$).

We also considered the possibility that firing rates might be explained better by the weights that the monkeys gave to the shapes. To test this, we added a term to equation (9) to represent the difference between the assigned $\log LR$ and the subjective WOE:

$$y_n = a_n + b_n \log LR_n + c_n I_{\text{eye}} + d_n \Delta_n \quad \text{where } \Delta_n = \sum_{i=1}^n \text{subjective WOE}_i - \log LR_n \quad (10)$$

The null hypothesis, $d_n = 0$, asserts that the subjective WOE affects the LIP firing rate in a manner that is explained by the $\log LR$ assigned to the shapes.

To estimate the effect of individual shapes on LIP responses (Fig. 4), we isolated the change in firing rate from the ‘baseline’ level attained prior to presentation of the shape. The baseline firing rate was estimated from individual

trials using the average response over the 200 ms preceding the onset of the shape (that is, from the preceding epoch). We subtracted this baseline from the response after the onset of the shape, and averaged the resulting traces across the population of 64 neurons.

To determine whether intermediate levels of firing rate could be explained as mixtures of high and low firing rate states (Fig. 5b), in each epoch, we grouped the neural responses into quintiles based on the rank of logLR. For each cell in each epoch, we calculated five mean firing rates and their associated variances. In the mixture model, we assumed that the responses comprising the three intermediate quintiles represent mixtures of values drawn from the extreme quintiles, termed anchors, representing high and low states. The proportion of high and low samples in each of the mixtures was set to match the mean firing rate for each bin. We then calculated the expected variance based on these proportions (theoretical curves in Fig. 5b). In the non-mixture model, the variance was established by interpolating between the variances associated with the anchor distributions. This is equivalent to assuming a constant Fano factor for all the quintiles, consistent with the idea that the intermediate mean is not a mixture. For the graphs in Fig. 5b, we normalized the variances (from model and data) to the mean of the five sample variances, and we normalized the mean firing rates to the average of the five means. This places the point for the middle quintile near [1,1] on these plots. We then averaged these normalized values over all neurons. We used F statistics to compare the observed variance to the value predicted from the mixture model and to the predicted value from the non-mixture model. The P values reported in association with Fig. 5b are based on combined data from all neurons; data from single neurons support the trends in the figure but lack the power to reject mixture or non-mixture, or both. Note that this analysis is more sensitive than standard tests for bimodality. For example, Hartigan's dip test failed to reject unimodality of the distributions associated with intermediate quintiles in all epochs, including the delay period ($P > 0.9$, combined standardized responses).

Correlation between choice and neural response. To measure the relationship between trial-by-trial variation in LIP response and behavioural choice, we incorporated firing rate as an additional term in the logistic model that explains the monkeys' choices based on the shape combinations. Using a nested models approach, we begin with the successful account of behaviour using the definition of logLR in units referable to the target in the neuron's response field:

$$P_{\text{RF}} = \frac{10^Q}{1 + 10^Q} \quad \text{where } Q = \beta_0 + \beta_1 \log_{10} \frac{P(s_1, s_2, s_3, s_4 | \text{reward at } T_{\text{in}})}{P(s_1, s_2, s_3, s_4 | \text{reward at } T_{\text{out}})} \quad (11)$$

This would produce the same graph as Fig. 1b with a new ordinate, labelled 'Probability of T_{in} choice'. In each epoch, $n = 1$ to 4, we incorporated a term that reflects the firing rate of the neuron. This value is the residual error after fitting firing rate as a function of logLR and subjective WOE in the n th epoch, which we incorporated into an extended logistic model of choice:

$$P'_{\text{RF}} = \frac{10^{Q'}}{1 + 10^{Q'}} \quad \text{where } Q' = Q + \beta_2 r_n \quad (12)$$

where r_n is the residual error in the fit to equation (10) but without the eye movement term (that is, $c_n = 0$). The ratio β_2/β_1 in equations (11) and (12) furnishes an estimate of the effect that the variable discharge of a single neuron in a single trial has on choice, in units of bans per spikes per second, that cannot be explained by the stimulus.

Unless otherwise noted, fits were performed using the method of maximum likelihood. Standard errors on the estimated parameters (coefficients) were obtained using the Hessian matrix of the log likelihood. The parameter estimates and their s.e. values were used to construct t statistics to test the null hypotheses.

51. Robinson, D. A. A method of measuring eye movement using a scleral search coil in a magnetic field. *IEEE Trans. Biomed. Eng.* **10**, 137–145 (1963).
52. Hayes, A. V., Richmond, B. J. & Optician, L. M. A UNIX-based multiple process system for real-time data acquisition and control. *WESCON Conf. Proc.* **2**, 1–10 (1982).
53. Lewis, J. W. & Van Essen, D. C. Corticocortical connections of visual, sensorimotor, and multimodal processing areas in the parietal lobe of the macaque monkey. *J. Comp. Neurol.* **428**, 112–137 (2000).
54. Lewis, J. W. & Van Essen, D. C. Mapping of architectonic subdivisions in the macaque monkey, with emphasis on parieto-occipital cortex. *J. Comp. Neurol.* **428**, 79–111 (2000).
55. Van Essen, D. C. *et al.* Mapping visual cortex in monkeys and humans using surface-based atlases. *Vision Res.* **41**, 1359–1378 (2001).
56. Bracewell, R. M., Mazzoni, P., Barash, S. & Andersen, R. A. Motor intention activity in the macaque's lateral intraparietal area. II. Changes of motor plan. *J. Neurophysiol.* **76**, 1457–1464 (1996).